scientific reports

Check for updates

OPEN

$NiCo_2O_4$ nanoparticles for enhancing voltammetric determination of sodium diclofenac in aqueous solutions

Luoana Florentina Pascu[1], Sorina Negrea[2], Sorina Motoc[3], Florica Manea[4]✉, Aniela Pop[4], Vasile-Adrian Surdu[5], Bogdan Stefan Vasile[6], Andreea Mădălina Pandele[7], Adelina-Carmen Ianculescu[6] & Raluca Dumitru[4]✉

The presence of the pharmaceuticals in water as emergent pollutants necessitates a continuous improving of their sensing, e.g., through voltammetric detection with the performance given by electrode composition. In this study, nickel cobaltite ($NiCo_2O_4$) synthesized by the thermolysis was deeply investigated by X-ray diffraction, high-resolution scanning electron microscopy (HR-SEM), and high-resolution transmission electron microscopy coupled with selected area electron diffraction. Also, X-ray photoelectron spectroscopy was used to determine the oxidation state of Ni and Co cations. $NiCo_2O_4$ was tested as modifier for commercial glassy carbon (GC) electrode by drop-casting as $NiCo_2O_4$/GC electrode for the voltammetric detection of sodium diclofenac salt (DCF) in water. In our study, the lowest limit of detection of 3 nM, better than ones reported in the literature, was achieved for DCF determination using differential pulse voltammetry with the scan rate of 0.05 V s^{-1}, step potential of 50 mV, modulation amplitude of 200 mV. The optimized voltammetric detection method was validated by DCF determination in real tap water.

Keywords Sodium diclofenac salt, Emerging pollutant, Advanced voltammetric detection, $NiCo_2O_4$ nanomaterials, Water monitoring

Currently, the spinel-type oxides have received growing attention due to their diversity and specific optical[1–3], magnetic[4], electrical[5] and chemical properties[6,7], which gives them high potential for various applications, e.g., chemical sensors[8], electronic devices[9], degradation processes[10], ecological pigments[11], anti-corrosion[12] etc. The $NiCo_2O_4$ spinel-type oxides have been proven to be active and stable bifunctional electrocatalysts for O_2 evolution and reduction in alkaline medium, characterized by better electronic conductivity (at least two orders of magnitude) and higher electrochemical activity than single nickel or cobalt oxides[13–15]. In general, electrochemical behavior of $NiCo_2O_4$ has been investigated for various applications, e.g., high performance supercapacitors[16], electrocatalysts for oxygen evolution[17], organic synthesis electrodes[18] and electrocatalyst characterized by high biocompatibility and low cost[19–22].

Recently, the interest for integrating spinel oxide-based nanostructures within the voltametric and amperometric detection has increased due to their advantages, e.g., chemical stability, superior electrocatalytic activity and low cost[23]. Very good performances related to the lowest limit of detection (LOD) have been reported for the voltametric detection using differential pulse voltammetry (DPV), such as: 150 nM for chloramphenicol detection using $ZnCo_2O_4$ nanoparticles modified screen-printed carbon electrode[24], 290 nM for paracetamol

[1]National Research and Development Institute for Industrial Ecology (INCD ECOIND), Drumul Podu Dambovitei Street No. 57-73, 060652 Bucharest, Romania. [2]National Institute of Research and Development for Industrial Ecology (INCD ECOIND), Bujorilor Street No. 115, 300431 Timisoara, Romania. [3]"Coriolan Drăgulescu" Institute of Chemistry, Romanian Academy, 24 Mihai Viteazu Bvd., 300223 Timisoara, Romania. [4]Polytehnic University of Timisoara, V. Parvan 6, 300223 Timisoara, Romania. [5]Department of Materials Science, Faculty of Materials Science and Engineering, Transilvania University of Brasov, 29 Eroilor Blvd., 500036 Brasov, Romania. [6]Department of Oxide Materials Science and Engineering, Faculty of Chemical Engineering and Biotechnologies, Polytechnic University of Bucharest, Gh. Polizu Street No. 1-7, 011061 Bucharest, Romania. [7]Department of Analytical Chemistry and Environmental Engineering, Faculty of Chemical Engineering and Biotechnologies, Polytechnic University of Bucharest, Gh. Polizu Street No. 1-7, 011061 Bucharest, Romania. ✉email: florica.manea@upt.ro; raluca.voda@upt.ro

detection using $ZnFe_2O_4$ nanoparticles modified screen-printed carbon electrode[23], 10 nM and 60 nM for simultaneous detection of morphine and diclofenac using $MgFe_2O_4$/graphite paste electrode[25]. Also, $NiCo_2O_4$ nanoflowers modified glassy carbon electrode allowed reaching LOD of 990 nM for nitrite detection using chronoamperometry[26].

Diclofenac is a non-steroidal anti-inflammatory drug that belongs to a class of emerging pollutants in water due to its poor (bio)degradation and widespread use, which causes unpredictable and adverse effects in the ecosystem[27]. The concentration levels of DCF and its metabolites have been reported in water in many countries, e.g., 170–2550 ng L^{-1} in Germany, 15–40 ng L^{-1} in Romania[28], and various types of water bodies, e.g., 2.40–140 ng L^{-1} in drinking water, 1.80–181 µg L^{-1} in the influent and 1.20–24.3 µg L^{-1} in the effluent of the wastewater treatment plants, and 3.90–14 ng g^{-1} in sediment-river/stream[29]. Thus, there is a demand for the development of simple, low-cost, environmentally friendly and in-situ analytical methods for the detection of DCF in water. Several conventional techniques have been conducted to determine the DCF in aqueous solution, i.e., spectrophotometry[30] spectrofluorimetry, high-performance liquid chromatography[31], gas chromatography–mass spectrometry[32], thin layer chromatography[33] and electrochemical analyses[29,34]. In general, conventional methods are robust and accurate, requiring expensive equipment and long analysis time, while electrochemical methods offer fast response, high sensitivity, specificity, low LOD, low cost, user-friendly operation and simplicity[35,36]. Also, the electrochemical methods are versatile and can be integrated into miniaturized and portable instruments. In addition, other advantages of electrochemical sensors are given by ability for in situ analysis, easy installation due to the small size of the equipment, fast response, simple and no sample preparation demand[37–39].

It is well-known that the electrode material is the core element for the electroanalysis efficacy using electrochemical sensors. Carbon-based electrodes have been the most commonly used[40], but their main limitations are given by slow kinetics reactions that can be enhanced more or less through carbon nanostructuring[41,42] or other modifications. Electrode composition can be modified through various compounds and methods to provide the electrocatalytic activity towards the detection of specific analytes via electrooxidation and/or electroreduction processes at certain electrode potentials, thereby enhancing sensitivity[43,44]. Additionally, the advanced electrochemical techniques, such as DPV and SWV, should be exploited to enhance the electroanalytical performance linked to the electrode features. Several electrode materials have been reported for the electrochemical detection of DCF, e.g., electrochemically activated carbon paste electrodes and multi-walled carbon nanotubes paste electrodes achieving the LOD of 0.29 µM DCF and respective, 0.001 µM DCF[45], modified electrodes based on attapulgite clay mineral with the LOD of 0.053 µM DCF[46], feather-type La^{3+}–ZnO nano-flower modified carbon paste electrode that get the LOD of 5.0 µM DCF[47] and diacerein modified carbon paste electrode with the LOD of 0.2 mM DCF[48].

In this context of modified electrode for sensing, synthesis of $NiCo_2O_4$ nanoparticles by the calcination of the precursor at 450 °C for at least 1 h including their advanced characterization, was studied in this work fortheir testing as electrocatalysts in DCF detection to improve its LOD. The electrochemical behavior of $NiCo_2O_4$, including the presence of redox systems as modifier of commercial GC electrode material, was studied towards DCF oxidation and reduction to assess their electrocatalytic activity in the development of advanced electrochemical detection of DCF in water. To the best of our knowledge, no study related to DCF detection using $NiCo_2O_4$/GC electrode material has been reported. The advanced DPV and SWV techniques were exploited, and their operating conditions were optimized for enhancing electrochemical detection of DCF including both its oxidation and reduction processes.

Materials and methods

Synthesis and characterization of $NiCo_2O_4$

The oxalate precursor was synthesized using $Ni(NO_3)_2{\cdot}6H_2O$, $Co(NO_3)_2{\cdot}6H_2O$, 1,2-ethanediol, and 2 M HNO_3 solution as reagents from Merck (Darmstadt, Germany). An aqueous solution with pH = 1 containing 1,2-ethanediol, $Ni(NO_3)_2{\cdot}6H_2O$, $Co(NO_3)_2{\cdot}6H_2O$, HNO_3 in the ratio of 3:1:2:1 was used. The reaction mixture was heated in a thermostat at 100 °C for about 40 min to generate $NiCo_2(C_2O_4)_3(OH_2)_4{\cdot}H_2O$ coordination compound that was further subjected to the thermolysis at 400 °C to obtain $NiCo_2O_4$ oxide.

Fourier-transform infrared (FTIR) spectrum of the precursor oxalate was recorded in the range of 4000–400 cm^{-1} on a Jasco FT-IR spectrophotometer (Jasco, Tokyo, Japan). TG (thermal gravimetry), DTG (differential thermogravimetry) and DSC (differential scanning calorimetry) curves were recorded on the precursor with a NETZSCH-STA 449C instrument (Netzsch Group, Selb, Germany) in the range of 25–700 °C, with a heating rate of 10 K min^{-1}.

X-ray diffraction (XRD) measurements were performed at room temperature using a Rigaku Ultima IV diffractometer (Rigaku Co., Tokyo, Japan), operating in a Bragg–Brentano configuration with Ni-filtered Cu-Kα (λ = 1.5406 Å) radiation. Phase identification was performed using HighScore Plus 3.0e software, connected to the ICDD PDF-4+ 2023 database. Lattice parameters were refined by the Rietveld method.

In order to investigate the morphology of the $NiCo_2O_4$ powder, high-resolution scanning electron microscopy (FE-SEM) investigations were performed by means of a FEI QUANTA INSPECT F50 microscope (FEI, Hillsboro, OR, US) with field emission gun. Morphological and structural details of the starting nanoparticles were also analyzed by transmission electron microscopy (TEM) and high-resolution transmission electron microscopy (HRTEM) coupled with selected area electron diffraction (SAED) with a TecnaiTM G^2 F30 S-TWIN transmission electron microscope (FEI, Hillsboro, OR, USA) operating at 300 kV. The particle size distribution of the $NiCo_2O_4$ powder was determined from the statistical analysis carried out by means of the OriginPro 9.0 software (OriginLab, Northampton, MA, USA). Size measurements on 60 isolated particles (from images of appropriate magnifications obtained from various microscopic fields) performed by means of the software Digital Micrograph 1.8.0 (Gatan, Sarasota, FL, USA) of the electron microscope, were accounted to determine average

particle size. Elemental energy dispersive X-ray (EDX) analysis was performed using a Titan Themis ultra-high-resolution electron microscope from Thermo Fisher Scientific (Hillsboro, OR, USA). For the acquisition of the elemental maps, the microscope was operated in STEM (Scanning transmission electron microscopy) mode at 300 kV using a HAADF (high-angle annular dark-field) detector for imaging and in column windowless 4 Super EDX detector for elemental analysis.

In order to establish the oxidation state of Ni and Co cations, X-ray photoelectron spectroscopy (XPS) investigations were carried out. The XPS spectra were acquired on a K-Alpha XPS spectrometer (Thermo Scientific), fitted with a monochromatic Al Kα source (1486.6 eV). Surface charging was compensated by a flood gun and binding energies were referenced to the C1*s* peak which was set at 284.6 eV. The pass energy for the high-resolution spectra was 20 eV. The deconvolution of core-level spectra was performed with mixed Gaussian–Lorentzian functions after subtracting a Shirley background.

Testing $NiCo_2O_4$/GC in electrochemical detection experiments

All the electrochemical experiments were performed using a classical three-electrode cell consisted of the platinum counter-electrode, the saturated calomel (SCE) reference electrode and the $NiCo_2O_4$ modified-GC ($NiCo_2O_4$/GC) working electrode connected to an Autolab Pontentiostat/Galvanostat PGStat 302 (EcoChemie, Utrecht, The Netherlands) controlled with GPES 4.9 software (EcoChemie, Utrecht, The Netherlands). The $NiCo_2O_4$/GC electrode was obtained by drop casting using 5 mg mL^{-1} $NiCo_2O_4$ suspension prior to each series of the electrochemical experiments. After 15 s of the GC electrode immersion and drying 15 min in the oven at a temperature of 70 °C, 10 continuous repetitive cyclic voltammograms (CVs) within − 1.00 V → + 1.00 V potential range running from 0.00 to + 1.00 and backward to − 1.00 V versus SCE were applied for the electrochemical stabilization of the electrode surface. The immersion time was set-up based on CV shape recorded in 0.1 M sodium hydroxide (NaOH) supporting electrolyte that was chosen to achieve the best electrocatalytic activity of $NiCo_2O_4$. For comparison, unmodified GC was subjected to the similar electrochemical experiments by CV. The experiments were performed in 0.1 M NaOH supporting electrolyte using voltammetric techniques, i.e., cyclic voltammetry (CV), SWV and DPV. CV was performed at various scan rates from 10 to 200 mV s^{-1}. SWV was performed with the scan rate of 0.5 V s^{-1}, step potential (SP) of 50 mV, modulation amplitude (MA) of 100 mV and frequency of 10 Hz. SP of 50 mV and MA ranged from 50 to 200 mV were used for DPV.

The relative standard deviation (RSD), limit of detection (LOD), and limit of quantification (LOQ) were calculated for three replicates using the following equations[49]:

$$\overline{x} = \frac{\sum_{i=1}^{n} x_i}{n} \tag{1}$$

$$S = \sqrt{\frac{\sum_{i=1}^{n} \left(|x_i - \overline{x}|^2\right)}{n-1}} \tag{2}$$

$$RSD = \frac{S}{\overline{x}} \tag{3}$$

$$LOD = \frac{3S}{m} \tag{4}$$

$$LOQ = \frac{10S}{m} \tag{5}$$

where $\overline{x}$ represents the mean value of the replicates, S is the standard deviation, RSD is the relative standard deviation, LOD is the limit of detection, LOQ is the limit of quantification, and m is the sensitivity coefficient obtained from the analysis.

The stock solutions of 0.3 mM DCF and 0.3 mM capecitabine (CCB) were daily prepared from analytical grade reagent (Sigma Aldrich) with double distilled water. The stock solution of 0.5 mM ibuprofen sodium salt (IBP) was prepared using 0.1 M NaOH solution. The real tap water samples were prepared by adding NaOH powder to achieve 0.1 M NaOH and spiked with known DCF concentrations (0.200 and 0.400 mg L^{-1} DCF). Above-mentioned similar protocol for the electrode stabilization was applied.

Results and discussion

Characterization of $NiCo_2O_4$ precursor

The $NiCo_2O_4$ precursor, oxalate coordination compound, was synthesized through the oxidation of 1,2-ethanediol with nitrate anion in accordance with reaction (6):

$$\begin{aligned} &3C_2H_4(OH)_2 + \left(\left[Ni(OH_2)_6\right]^{2+} + 2NO_3^-\right) + 2\left(\left[Co(OH_2)_6\right]^{2+} + 2NO_3^-\right) + 2\left(H^+ + NO_3^-\right) \\ &\xrightarrow{\Delta t^\circ} NiCo_2(C_2O_4)_3(OH_2)_4 \cdot H_2O_{(s)} + 8NO_{(g)} + 23H_2O_{(g)} \end{aligned} \tag{6}$$

and it was characterized by IR spectrum (Fig. S1, SM). All IR absorption bands characteristic to oxalate ligand with the corresponding assignments are gathered in Table 1.

The ligand oxalate is bidentate [1626 cm^{-1} ($\nu_{asym\ O=C-O^-}$), 1317 cm^{-1} ($\nu_{sym\ O=C-O^-}$] and tetradentate [1385 cm^{-1} ($\nu_{asym\ OCO^-}$), 1360 cm^{-1} ($\nu_{sym\ OCO^-}$), 922 cm^{-1} (δ_{OCO^-})][44,50]. The band at 490 cm^{-1} confirmed the coordination of oxalate ligand[51]. The thermal decomposition of the oxalate precursor (Fig. S2, SM) in

Wavenumber (cm^{-1})	Assignment
3389	ν(OH) from coordinated water
1626	ν_{asym} (O=C–O$^-$)
1385	ν_{asym} (OCO$^-$)
1360	ν_{sym} (OCO$^-$) + ν(C–C)
1317	ν_{sym} (O=C–O$^-$)
1076	$\nu_{(C-O)}$
922	δ(OCO$^-$)
824	Lattice water
490	ν(M–O)

Table 1. IR absorption bands characteristic for oxalate ligand and the corresponding assignments.

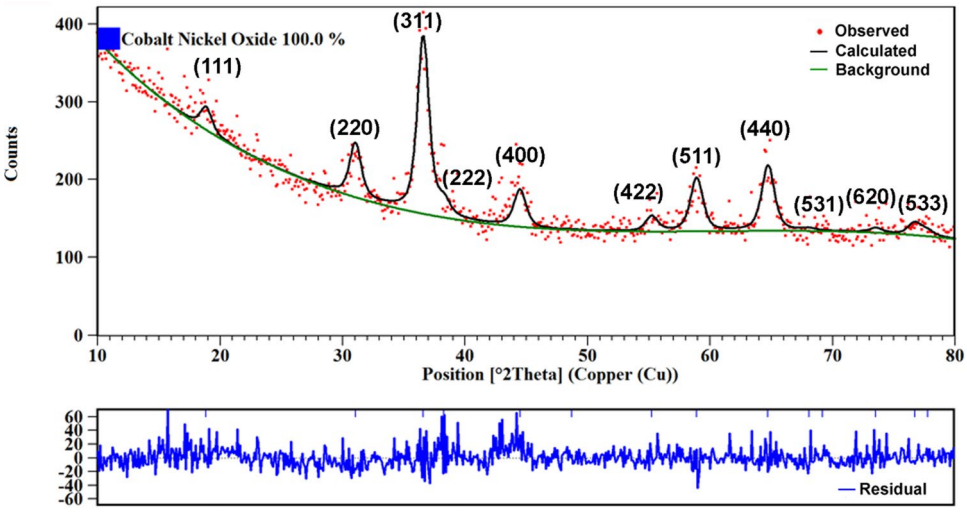

Fig. 1. XRD pattern at room temperature with Rietveld refinement of the $NiCo_2O_4$ powder under investigation.

air atmosphere shows the formation of $NiCo_2O_4$ as end decomposition product (mass loss calcd./found (%): 54.67/54.33). The first decomposition step of the coordination compound characterized by an endothermic effect shows removal of the lattice water (25–160 °C, mass loss: found 3.20%; calcd. 3.39%). The second decomposition step (160–250 °C) characterized by an endothermic effect is attributed to the loss of the coordinated water molecules (mass loss: found 12.98%; calcd. 13.57%). In the third decomposition step (250–450 °C), the exothermic effect is assigned to the degradation of the oxalate anions (mass loss, found 38.15%, calcd. 37.71%) but also to the partial oxidation of M(II) to M(III) with obtaining of spinel $NiCo_2O_4$ compound.

Characterization of the $NiCo_2O_4$ nanoparticles

Phase composition and crystal structure

The XRD pattern recorded at room temperature shows a single-phase composition, $NiCo_2O_4$ with spinel structure being the unique crystalline compound identified with the ICDD card no. 04-018-4105 (Fig. 1).

The structural characteristics and the fitting parameters obtained by the Rietveld refinement are listed in Table 2.

These results indicate a single-phase of $NiCo_2O_4$ spinel oxide characterized by cubic crystal systems with crystallite size bellow 10 nm.

Morphology, crystallinity and chemical homogeneity

FE-SEM investigations performed in order to notice the size, morphology and agglomeration tendency of the $NiCo_2O_4$ particles show the formation of almost spherical aggregates of various sizes ranged between 160 and 300 nm, as the lower magnification image reveals (Fig. S3a, SM). The higher magnification image of Fig. S3b (SM) shows a structuring of these aggregates, which seem to consist of very small primary particles, most likely in the nanometer range, whose sizes are very difficult to be determined. The large-area EDX mapping indicates an uniform distribution of Ni and Co species (Fig. S3c, SM), reflected in the lack of any Ni- and/or Co-rich secondary phases and thus sustaining the XRD data.

To estimate an average particle size and the crystallinity degree such small particles TEM/HRTEM analyses are required. TEM images of Fig. 2a and b show that the $NiCo_2O_4$ powder consists of uniform (as size and shape)

Characteristics	$NiCo_2O_4$ powder
Crystal system/space group	Cubic/Fd-3m
Lattice parameter, a [Å]	8.136973 ± 0.008899
Unit cell volume, V (Å^3)	538.7517
Structural density, $<\rho_s>$ (g/cm^3)	5.93
Crystallite size, $<D>$ (nm)	6.25 ± 0.24
Micro strain, $<S>$ (%)	1.56 ± 0.77
R expected, R_{exp}	10.0807
R profile, R_p	5.4257
Weighted R profile, R_{wp}	7.3423
Goodness of fit, χ^2	0.5305

Table 2. Structural characteristics of the $NiCo_2O_4$ under investigation.

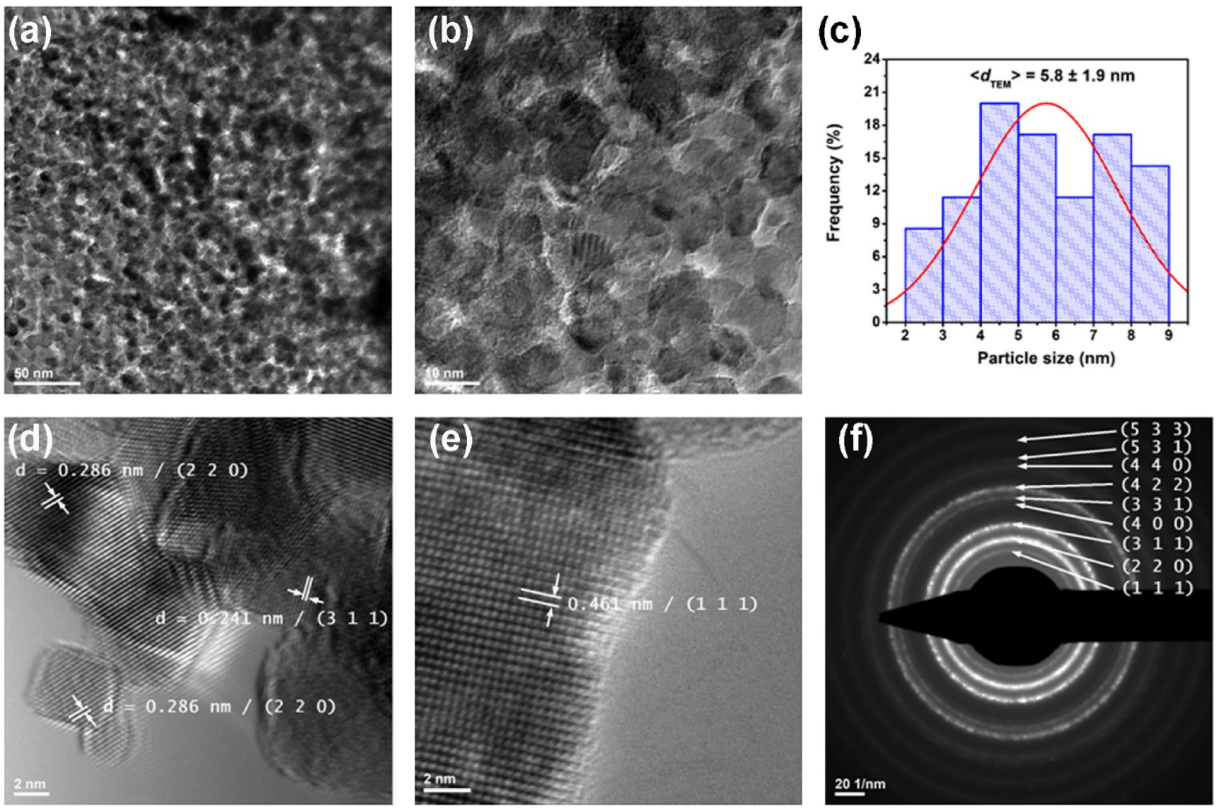

Fig. 2. TEM images of various magnifications. (**a**,**b**) histogram showing the particle size distribution. (**c**–**e**) HRTEM images. (**f**) SAED pattern of the $NiCo_2O_4$ nanoparticles.

nanoparticles, with sizes below 10 nm and with a high agglomeration tendency. A narrow, unimodal particle size distribution, with an estimated average particle size of (5.8 ± 1.9) nm was found, as revealed the histogram of Fig. 2c. Comparing the average crystallite size determined from the XRD data and the average particle size estimated from TEM investigations and taking into account the error bars, it can conclude that the nanoparticles are single crystals.

The HRTEM images of Fig. 2d and e indicate a well-faceted polyhedral shape with well-defined edges and rather rounded corners of the nanoparticles. Despite their small size, the nanoparticles show a high crystallinity degree proved by the parallel ordered fringes observed in the HRTEM images (Fig. 2d,e), as well as by the well-marked concentric diffraction rings, specific to the crystalline planes of the spinel structure, in the corresponding SAED pattern (Fig. 2f).

In order to check the chemical homogeneity at the local scale, EDX investigations in the STEM mode on the area indicated in Fig. S4a (SM) were also performed. The elemental maps of Co, Ni and O (Fig. S4b–d, SM), as well as the global map resulted by the superposition of the all three elemental maps (Fig. S4e, SM) indicate a high chemical homogeneity proved by the uniform distribution of Co and Ni cations inside the aggregates of $NiCo_2O_4$ nanoparticles. The EDX spectrum depicted in Fig. S4f points out, apart from the peaks specific to the

carbon and copper species related to the TEM grids, the presence only of the peaks characteristic to the species Ni, Co, O which compose the $NiCo_2O_4$ nanoparticles, this demonstrating the high purity of the spinel powder.

XPS investigations

The samples were further characterized by high resolution XPS in order to estimate the surface chemistry of $NiCo_2O_4$ nanopowder and to distinguish the valence state of the Ni and Co cations using binding energies (BE). The survey spectrum depicted in Fig. 3a shows the presence of Ni, Co, O elements. In accordance to Fig. 3b, two spin–orbit doublets at 873.1 and 855.9 eV were present in the high-resolution Ni 2*p* XPS spectrum, along with two clearly visible shakeup satellites that correspond to Ni $2p_{1/2}$ and Ni $2p_{3/2}$ signals, respectively[52,53]. At a close examination, deconvolution of Ni $2p_{3/2}$ peak illustrates the presence of two different energy band types at 855.2 eV attributed to Ni^{2+}, and at 857.1 eV assigned to Ni^{3+}. The Co 2*p* spectrum shown in Fig. 3c is comparable to the Ni 2*p* spectrum in that it has two spin–orbit coupling energy levels, $2p_{3/2}$ and $2p_{1/2}$, at 795.4 and 780.1 eV[54]. The deconvolution of the Co $2p_{3/2}$ peak indicates the presence of both Co^{3+} and Co^{2+} species identified by their specific energy bands located at 779.8 eV and 781.2 eV. Besides, satellite peaks located at 861.7 and 880.1 eV, in the case of Ni 2*p* and 789.3 and 797.0 eV for the Co 2*p* were also noticed in the corresponding XPS spectra[55].

From these results one can conclude that, if we assume that $NiCo_2O_4$ is a typical inverse spinel, its formula can be written as

$$\left(Co^{+3}_{1-x}Co^{+2}_{x}\right)_{Td}\left(Co^{+3}Ni^{+2}_{1-x}Ni^{+3}_{x}\right)_{Oh}O_4, \tag{7}$$

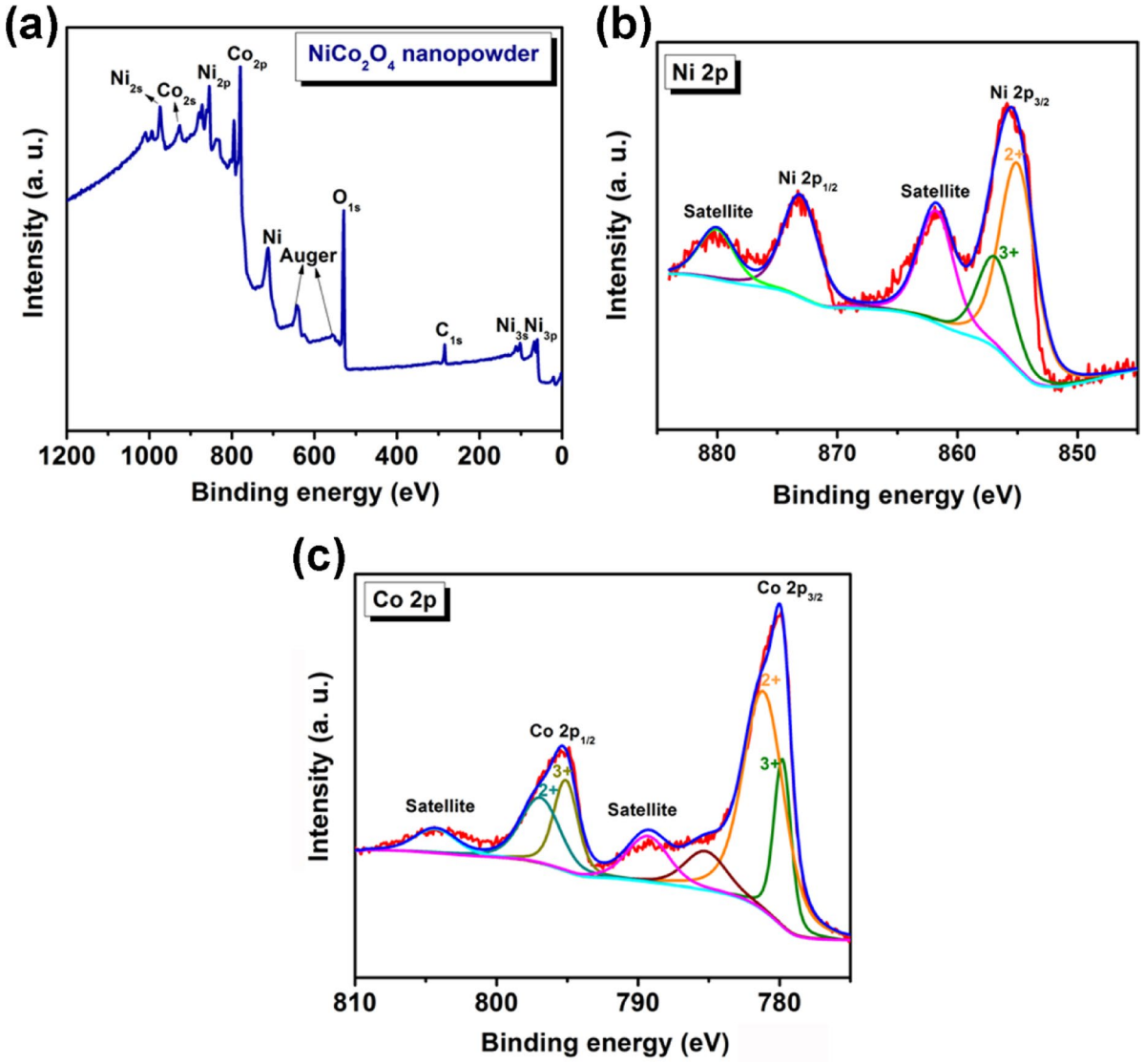

Fig. 3. High resolution XPS spectrum of $NiCo_2O_4$ powder. (**a**) Survey spectrum. (**b**) BE range corresponding to Ni 2*p* states. (**c**) BE range corresponding to Co 2*p* states.

with Ni cations placed exclusively on octahedral sites, irrespective of their oxidation state, and Co species occupying octahedral sites as Co^{3+} and both tetrahedral and octahedral sites as Co^{2+}[56]. However, it is worthy to mention that more recent theoretical studies[57,58] shown that intermediate states (see formula (7)), resulting due to the Co and Ni exchange between tetrahedral and octahedral sites and defined by the so-called "degree of inversion", *x*, should also be taken into account (formula (8)).

$$(\mathrm{Co_xCo_{1-x}})_{\mathrm{Td}}\,(\mathrm{Co_{2-x}Ni_x})_{\mathrm{Oh}}\,\mathrm{O_4} \quad (0 \le x \le 1) \tag{8}$$

It was found that the inversion degree strongly depends on temperature and preparation method. Based on their DFT study, Chang et al.[59], provides a new insight regarding the relationship between the degree of inversion and some physical properties as oxidation state, electronic structure and band structure in $NiCo_2O_4$, while Ndione et al.[57], reported a method to control the electrical properties of $NiCo_2O_4$ by manipulating the degree of inversion.

$NiCo_2O_4$/GC characterization and application in electrochemical sensing of sodium diclofenac in aqueous solutions

The presence of $NiCo_2O_4$ nanoparticles is characterized by non-uniform dispersion on the GC surface. Electroactive surface area determined by classical ferry/ferro redox system generated by CV in the presence of 4 mM $K_3[Fe(CN)_6]$ in 1 M KNO_3 supporting electrolyte at different scan rates is 0.035 cm^2 versus geometrical one of 0.031 cm^2.

Cyclic voltammetry

CV was first applied to investigate the electrocatalytic effect of $NiCo_2O_4$ spinel type oxide towards the electrooxidation of sodium diclofenac in alkaline media (0.1 M NaOH) by recording CVs comparatively on $NiCo_2O_4$/GC and simple GC electrodes. Also, 0.1 M Na_2SO_4 supporting electrolyte (considering the real matrix of water) was tested but no stable response was achieved (this result is not shown in the manuscript). Figure S5a and b (SM) present CVs recorded in 0.1 M NaOH supporting electrolyte within the potential range from 0 to + 1.00 V/SCE and back to − 1.00 V/SCE at the scan rate of 0.05 V s^{-1} in the absence (curve 1) and presence of 17 µM DCF (curve 2) on $NiCo_2O_4$/GC and GC electrodes, respectively. It is obvious that the presence of $NiCo_2O_4$ on GC modified the CV shape in 0.1 M NaOH through the appearance of two anodic peaks at the potential values of + 0.20 V/SCE (a1) and + 0.45 V/SCE (a2), respectively. These peaks can be assigned to the redox couples of Ni (II)/Ni (III) and/or Co (II)/Co(III) and Co(III)/Co(IV) and/or Ni (III)/Ni (IV) based on the literature[60–62] and modified considering proposed formulas of inverse spinel[7,8] in accordance with reactions (9–12):

$$\text{For x} = 0, \quad \mathrm{Ni^{+2}Co_2^{+3}O_4^{-2}} + \mathrm{OH^-} + \mathrm{H_2O} \rightarrow \mathrm{Ni^{3+}OOH} + 2\mathrm{Co^{3+}OOH} + \mathrm{e^-} \tag{9}$$

$$\text{For x} = 1, \quad \mathrm{Ni^{+3}Co^{+2}CO^{+3}O_4^{-2}} + \mathrm{OH^-} + \mathrm{H_2O} \rightarrow \mathrm{Ni^{3+}OOH} + 2\mathrm{Co^{3+}OOH} + \mathrm{e^-} \tag{10}$$

$$\mathrm{Co^{3+}OOH} + \mathrm{OH^-} \rightarrow \mathrm{Co^{+4}O_2} + \mathrm{H_2O} + \mathrm{e^-} \tag{11}$$

$$\mathrm{Ni^{3+}OOH} + \mathrm{OH^-} \rightarrow \mathrm{Ni^{+4}O_2} + \mathrm{H_2O} + \mathrm{e^-} \tag{12}$$

Also, it has been reported that higher valence oxides/hydroxides of cobalt can be generated within the potential range from + 0.37 to + 0.45 V[63]. On the CV backward, only one clear cathodic peak (c_1) is noticed at the potenial value of + 0.25 V/SCE, which can be result of overlapping of the Co (IV)/Co(III) and Ni (III)/Ni (II) pairs redox peaks. In the presence of DCF, the first peak current of $NiCo_2O_4$/GC decreased, probably due to DCF sorption process, but a higher second current peak (a_2) is generated, which is ascribed to the DCF oxidation, indicating the good electrocatalytic activity of $NiCo_2O_4$/GC. It is supposed that the DCF is oxidized into by-product while NiOOH and Co(IV) are reduced into $Ni(OH)_2$ and Co(III), respectively, in accordance with the literature data[64].

The electrochemical behavior of DCF on GC electrode exhibited the appearance of slight anodic current peaks at the potential values of − 0.150 V/SCE (a_1') and + 0.035 V/SCE (a_2'), indicating DCF oxidation in two steps involving carbon oxidation.

The useful signals recorded for 17 µM DCF onto both electrodes and presented in Table 3, showed significant higher sensitivity in the presence of $NiCo_2O_4$ (e.g., 84.3 vs. 0.059 µA $µM^{-1}$ cm^{-2}), proving the electrocatalytic activity of $NiCo_2O_4$ towards DCF oxidation. Additionally, cathodic signal revealed the electrocatalytic activity of $NiCo_2O_4$ towards the reduction of DCF byproducts through Ni (III)/Ni (II) and/or Co(III)/Co(II) and respective, Ni (IV)/Ni (III) and/or Co(IV)/Co(III).

Electrode	E_{det}/V vs. SCE	ΔI (µA $µM^{-1}$ cm^{-2})	Signal type
$NiCo_2O_4$/GC	+ 0.480	84.3	Anodic
	+ 0.250	43.1	Cathodic
GC	− 0.150	0.159	Anodic
	0.035	0.059	Anodic

Table 3. Useful signal and detection potential for DCF determination.

To clarify some detection related mechanistic aspects for the DCF oxidation and reduction onto $NiCo_2O_4$/GC electrode, the influence of the scan rate was investigated within the range from 10 to 200 mV s^{-1} in 0.1 M NaOH and the absence/presence of 17 µM DCF (Fig. 4a,b).

As shown in inset of Fig. 4a, the first anodic peak current (a_1) assigned to Ni(II)/Ni(III) redox couple is better evidenced at the low scan rate. However, it decreased with increasing scan rate and completely disappeared after a scan rate of + 0.300 V, indicating slow kinetics of this redox couple. The second anodic peak current (a_2) and the corresponding reduction cathodic peak current (c_1) increased linearly with the square root of the scan rate (Fig. S6a, SM), suggesting a diffusion-controlled step in the electrochemical behavior of $NiCo_2O_4$. Additionally, the potential of the anodic oxidation peak is shifted to a more positive direction and the cathodic reduction peak potential is shifted to a more negative direction with increasing the scan rate, which is characteristic of irreversibility (Fig. S6b, SM). However, considering the reversible character of each redox pair, this behavior is due to a complex mechanism that includes the potential generation of more oxides/hydroxide species and the overlapping of the Co(IV)/Co(III) and/or Co(III)/Co(II) and Ni(IV)/Ni(III) and/or Ni(III)/Ni(II) redox peaks. Also, the kinetics parameters of the redox process described by the anodic peak (a_2) and the corresponding cathodic peak (c_1) for the heterogeneous electron transfer were determined using the equations proposed by Laviron[65]. Thus, from the linearization of $\Delta E = Ep - E^{o\prime}$ versus the logarithm of scan rate, the transfer coefficient (α) and the apparent charge transfer rate constant (k_0) were determined. The slopes of the anodic and cathodic linearization, expressed by 2.3RT/αnF and 2.3 RT/(1 − α)n (13), allowed α determination as 0.40. Using the equation: $\log k_0 = \alpha \log(1-\alpha) + 1(-\alpha)\log\alpha - \log(RT/nFv) - \alpha\ 1(-\alpha)nF\Delta Ep\ 3.2/RT$ (14), the value of k_0 were determined as 0.378 s^{-1}.

One cathodic current peak was noticed at the potential value of − 0.450 V/SCE due to carbon reduction, which increased in the DCF presence. These anodic and cathodic current peaks are also manifested, on $NiCo_2O_4$/GC electrode, being assigned to carbon oxidation/reduction, and they slightly shifted to more negative value due to the presence of $NiCo_2O_4$. Additionally, in this cathodic range, negative currents occurred for anodic oxidation, which were not further considered for the detection.

The presence of 17 µM DCF did not affected the shapes of the CVs with increasing scan rate, except for the first anodic peak current (a_1), which disappeared after the scan rate of 0.02 V s^{-1}. This can be explained by the strong adsorption of DCF in this step. The slight influence of DCF presence is manifested by the higher slopes of the linear dependences of both anodic and cathodic currents versus the square root of the scan rates. This effect proves the diffusion-controlled step with faster kinetics of the overall DCF oxidation on the $NiCo_2O_4$/GC electrode, which is desired for the advanced electrochemical sensing. Based on the above-presented mechanistic aspects, corroborated with the literature data[66], the scheme of redox reaction mechanism of diclofenac oxidation involved in the anodic and cathodic detection is proposed in Fig. 5.

The effect of increasing DCF concentration within the concentration range from 3.4 to 34 µM DCF on the shape of CV recorded in 0.1 M NaOH supporting electrolyte on $NiCo_2O_4$/GC comparatively on GC electrodes is shown in Fig. 6a and b.

It is evident that after the initial step of DCF sorption, the further oxidation occurs at the potential value of + 0.480 V/SCE. During the CV backward scan, the corresponding cathodic current is lower. This behaviour indicates the Co(III)/Co(IV) and/or Ni(III)/Ni(IV) mediated DCF oxidation and the corresponding reduction of its oxidation by-product. Linear dependences of the anodic and cathodic peak currents versus DCF concentrations are noticed (Fig. 6c). Additionally, linear regressions of the anodic peak currents recorded on the GC electrode versus DCF concentrations (Fig. 6d) showed very low sensitivities reached with GC compared with $NiCo_2O_4$ (71.6 µA μM^{-1} cm^{-2} vs. 0.137 µA μM^{-1} cm^{-2}).

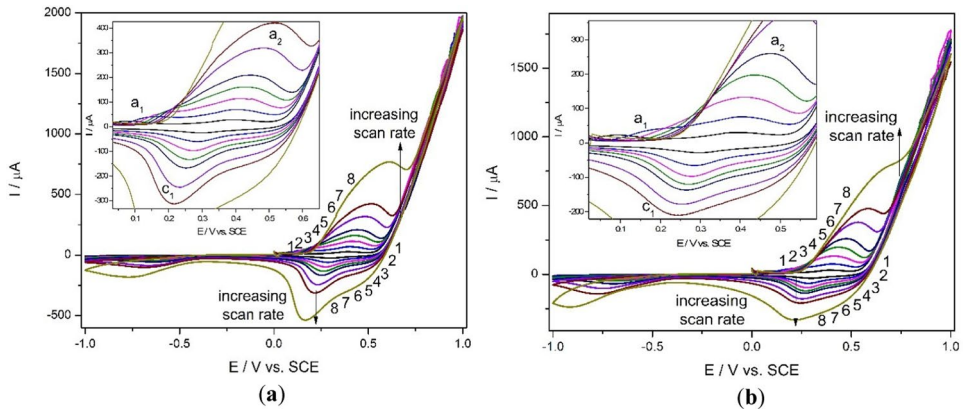

Fig. 4. Influence of the scan rate on CVs. (**a**) CVs recorded at $NiCo_2O_4$/GC electrode in 0.1 M NaOH supporting electrolyte at various scan rates: 10 mV s^{-1} (curve 1), 20 mV s^{-1} (curve 2), 30 mV s^{-1} (curve 3), 40 mV s^{-1} (curve 4), 50 mV s^{-1} (curve 5), 70 mV s^{-1} (curve 6), 100 mV s^{-1} (curve 7), 200 mV s^{-1} (curve 8). (**b**) CVs recorded at $NiCo_2O_4$/GC electrode in 0.1 M NaOH supporting electrolyte and 17 µM DCF at various scan rates: 10 mV s^{-1} (curve 1), 20 mV s^{-1} (curve 2), 30 mV s^{-1} (curve 3), 40 mV s^{-1} (curve 4), 50 mV s^{-1} (curve 5), 70 mV s^{-1} (curve 6), 100 mV s^{-1} (curve 7), 200 mV s^{-1} (curve 8).

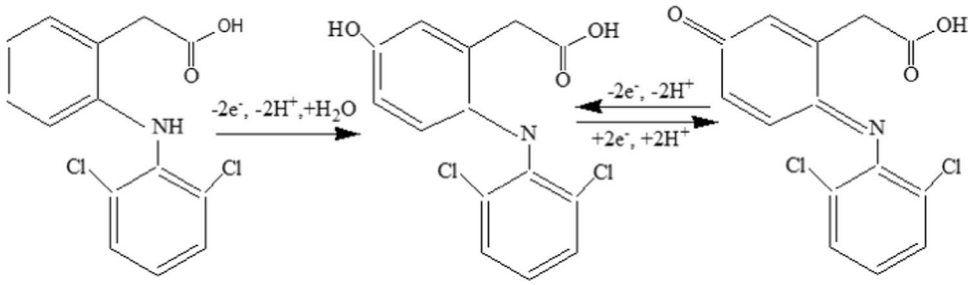

Fig. 5. Proposed mechanism for the electrooxidation of diclofenac.

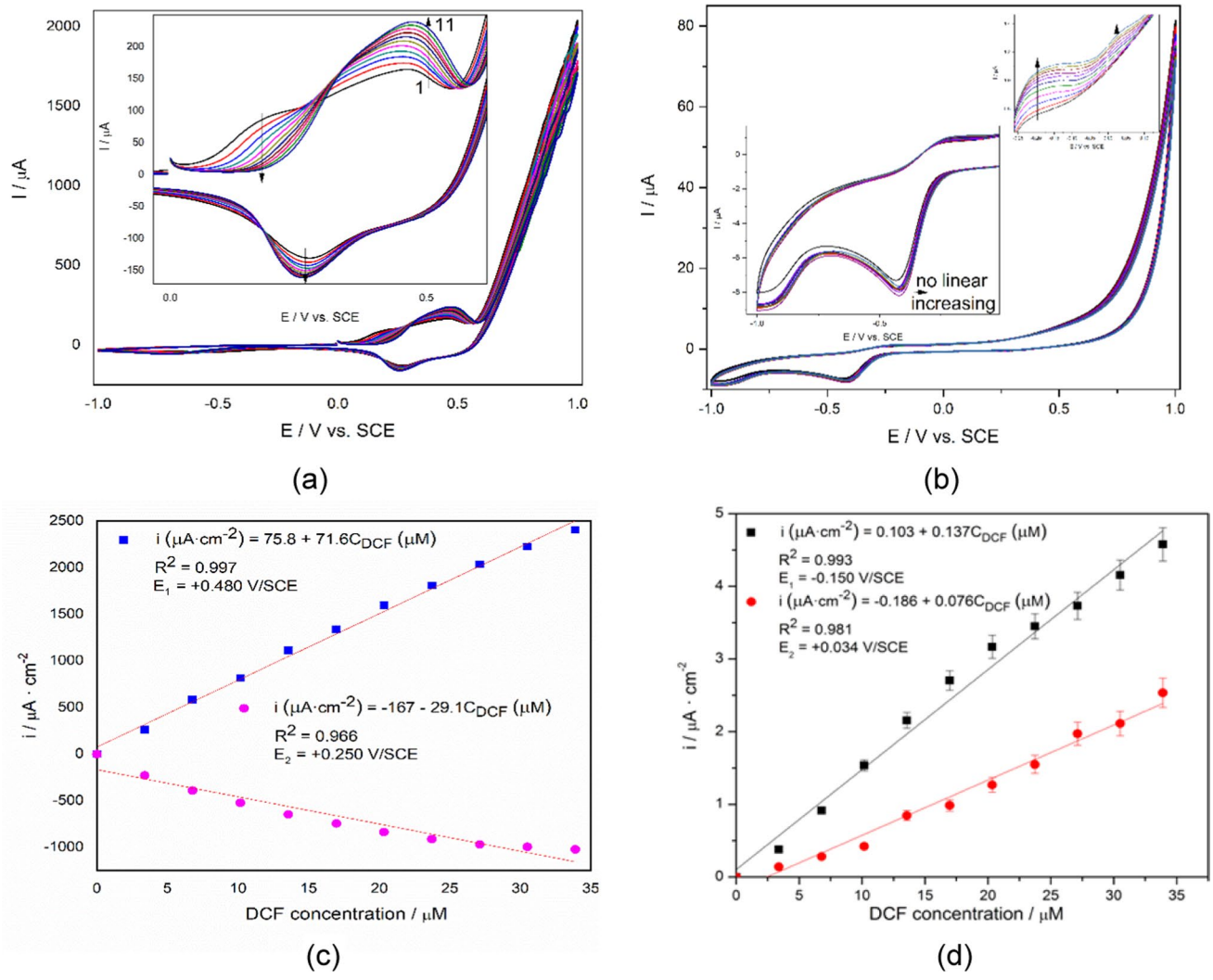

Fig. 6. CV-based detection results. (**a**) CVs recorded at the 0.05 V s^{-1} scan rate in 0.1 M NaOH supporting electrolyte and in the presence of various DCF concentrations ranged from 3.4 to 34 µM on the $NiCo_2O_4$/GC electrode. (**b**) CVs recorded at the 0.05 V s^{-1} scan rate in 0.1 M NaOH supporting electrolyte and in the presence of various DCF concentrations ranged from 3.4 to 34 µM on the GC electrode. (**c**) Calibration plots for DCF concentrations ranged from 3.4 to 34 µM on the $NiCo_2O_4$/GC. (**d**) Calibration plots for DCF concentrations ranged from 3.4 to 34 µM on the GC electrode.

Square-wave voltammetry (SWV) and differential-pulsed voltammetry (DPV)

Compared with CV, SWV provides faster and enhanced voltammetric signals due to its advanced features, which can be tuned through operating variables such as frequency, SP and MA. Figure 7a presents a series of SWVs recorded on $NiCo_2O_4$/GC electrode in 0.1 M NaOH with DCF concentrations ranging from 3.4 to 24 µM.

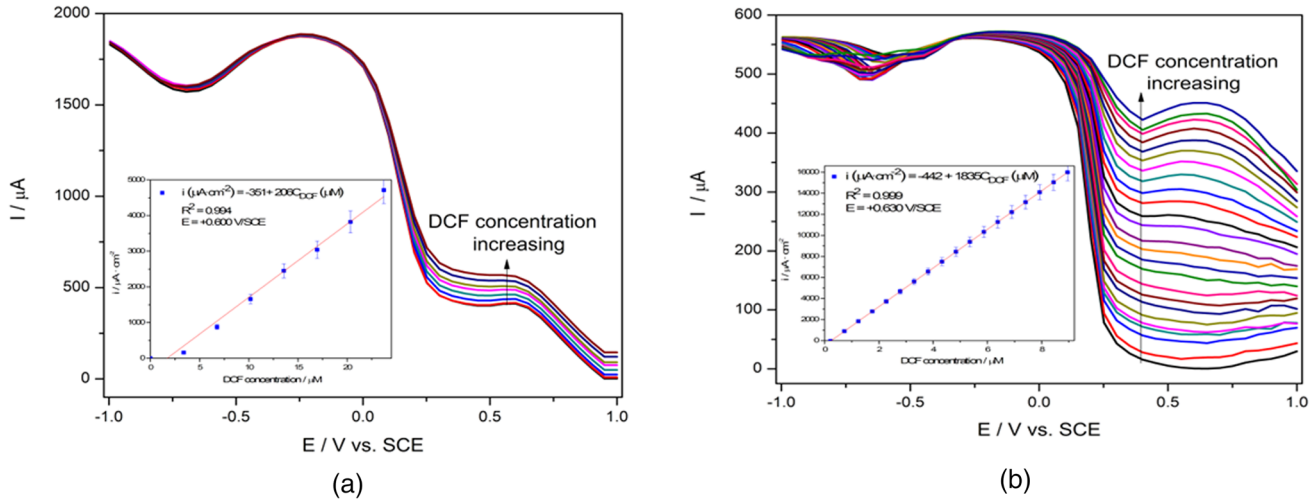

Fig. 7. (**a**) Square-wave voltammograms recorded on $NiCo_2O_4$/GC electrode in 0.1 M NaOH supporting electrolyte, in the presence of various DCF concentrations: 3.4–24 µM, SP of 50 mV, MA of 100 mV, f = 10 Hz. Inset: Calibration plots for DCF detection in the concentration range 3.4–24 µM recorded at the potential value of E = + 0.600 V/SCE. (**b**) Differential-pulse voltammograms recorded on $NiCo_2O_4$/GC electrode in 0.1 M NaOH supporting electrolyte, in the presence of various DCF concentrations: 0.34–8.14 µM, SP of 50 mV and MA of 100 mV. Inset: Calibration plots for DCF detection in the concentration range of 0.34–8.14 µM recorded at the potential value of E = + 0.630 V/SCE.

Technique	Working parameters	Detection potential (V/SCE)	Sensitivity (µA μM^{-1} cm^{-2})	LOD (µM)	LQ (µM)	R^2
CV	v = 0.05 V s^{-1}	+ 0.250 (cathodic signal)	29.1	0.100	0.360	0.966
		+ 0.480	71.6	0.022	0.075	0.997
SWV	v = 0.5 V s^{-1}	+ 0.600	206	0.004	0.014	0.994
	SP = 50 mV					
	MA = 100 mV					
	f = 10 Hz					
DPV	v = 0.05 V s^{-1}	+ 0.630	1835	0.004	0.014	0.999
	SP = 50 mV					
	MA = 100 mV					
	v = 0.05 V s^{-1}	+ 0.730	3057	0.003	0.010	0.971
	SP = 50 mV					
	MA = 200 mV					

Table 4. Analytical parameters achieved for $NiCo_2O_4$/GC electrode tested in DCF voltammetric detection.

The linear calibration of SWV currents recorded at + 0.600 V/SCE versus DCF concentrations showed a sensitivity of 206 µA μM^{-1} cm^{-2}, which is higher compared to CV recorded at the same scan rate. However, DPV technique was tested under various operational variables to substantially improve the voltammetric performance, considering its superiority in sensitivity, accuracy and resolution. The step potential (SP) was varied between 50 and 100 mV and the modulation amplitude (MA) ranged from 100 to 200 mV. The best results regarding the accuracy and the sensitivity were achieved with an SP of 50 mV and MA of 100 and 200 mV (Fig. 7b).

It can be noticed that the operating variables significantly impacted the voltammetric sensing performance. The lower MA allowed detection for a larger DCF concentration range while higher MA showed better sensitivity, which implicitly leads to better limit of detection. The electrochemical performance of the $NiCo_2O_4$/GC tested in this work is summarized in Table 4.

The lowest limit of detection of 3 nM achieved for DCF detection on $NiCo_2O_4$, which is better than those reported in the literature (see Table 5), demonstrates the great potential of this electrode for practical application in detecting DCF from aqueous solution.

The results of the interference study in DCF detection at $NiCo_2O_4$/GC electrode using optimized DPV and SWV in the presence of 24 µM ibuprofen from anti-inflammatory class and 14 µM capecitabine from cytostatic class shows that the response recorded at about + 0.600 V versus SCE is not affected (see example using SWV—Fig. S7, SM). Additionally, the presence of 1 mM chloride and 1 mM sulphate did not interfere with the DCF response. The reproducibility of the electrode using the optimized DPV technique was evaluated through three replicates measurements of 0.200 mg L^{-1} DCF. The relative standard deviation (RSD) of a maximum 1.50%

Method	Electrode	LOD (μM)	Refs.
DPV	Microporous Si_3N_4 membrane modified water-1,6-dichlorohexane interface system	1.5	[33]
DPV	Zn/Fe LDH-PANI	0.235	[30]
DPV	Activated graphite	0.29	[45]
	Graphite with nanotube	0.001	
SWV	GCE/AminoAT	0.204	[46]
	GCE/APTES-Amino-AT-Silica	0.053	
DPV	Feather-type La^{3+}–ZnO nano-flower modified carbon paste electrode	5.0	[47]
DPV	Diacerein modified carbon paste electrode	200	[48]
DPV	Magnesium ferrite $MgFe_2O_4$/graphite paste electrode	0.06	[25]
DPV	$NiCo_2O_4$/GC	0.003	This work

Table 5. Comparative performances for electrochemical sensing of DCF on $NiCo_2O_4$/GC electrode vs reported literature.

demonstrated the good reproducibility of the detection methods. A recovery test was performed by analyzing three parallel tap water samples spiked with 0.200 and 0.400 mg L^{-1} DCF. The minimum recovery values of 97% and the maximum RSD values of 2% for both concentrations demonstrated good recovery and reproducibility of the results. Finally, the results obtained using optimized DPV using were compared with those obtained by a conventional spectrophotometric method. Based on the obtained results, it can be concluded that the results of voltametric method are very close to spectrophotometric ones, revealing a good accuracy of the proposed voltammetric method.

Main limitations of this detection method should consider the interference of more complex matrices (e.g., wastewater) including the high organic loading, considering the potential of the fouling effect, as well as. Future work will be focused on the optimizing the composition of the $NiCo_2O_4$ based composite electrode including specific membranes for assuring the selectivity for DCF detection and avoiding the fouling effect.

Conclusions

$NiCo_2O_4$ nanoparticles with sizes bellow 10 nm characterized as inverse spinel oxide with single-phase composition and a cubic crystal system, were obtained after calcination of oxalate as $NiCo_2O_4$ precursor at 450 °C for at least 1 h. The electrocatalytic effect of $NiCo_2O_4$ nanoparticles towards sodium diclofenac detection was demonstrated using a $NiCo_2O_4$ modified glassy carbon electrode in comparison with the unmodified glassy carbon electrode (GC) electrode. The presence of nickel cobaltite on the surface of the GC electrode conferred the electrocatalytic activity for the DCF oxidation and reduction, mediated by complex redox couples of Ni(II)/Ni(III) and/or Ni(III)/Ni(IV) and Co(II)/Co(III) and/or Co(III)/Co(IV), considering the specific characteristics of inverse spinel oxide. Additionally, quasi-reversible complex reduction processes of DCF oxidation byproducts with lower kinetics compared to the oxidation process, involving overlapping redox pairs, were manifested. Square-wave and differential-pulse voltammetry techniques, through their specific characteristics, allowed for improved detection performance via DCF oxidation process. The best electroanalytical performances, with a sensitivity of 3057 μA μM^{-1} cm^{-2} and a detection limit of 3 nM, were obtained. However, the LOD of 4 nM achieved by SWV technique should be considered for very fast detection method (ten times faster than CV or DPV). The presence of 24 μM IBP from anti-inflammatory class and 14 μM CCB from cytostatic class, along with 1 mM chloride and 1 mM sulphate, did not interfere with the DCF response on $NiCo_2O_4$/GC electrode. Additionally, good reproducibility and accuracy were found for the voltammetric methods proposed for DCF detection. All results of electroanalytical performance for DCF detection, along with its flexibility for anodic and/or cathodic detection, indicate that the $NiCo_2O_4$/GC electrode has great potential for detecting of DCF in aqueous matrices.

Data availability

The dataset supporting the conclusions of this article is included within the article and supplementary material.

Received: 17 March 2025; Accepted: 17 June 2025
Published online: 03 July 2025

References

1. Addabbo, T. et al. Gas sensing properties and modeling of $YCoO_3$ based perovskite materials. *Sens. Actuators B* **221**, 1137–1155. https://doi.org/10.1016/j.snb.2015.07.079 (2015).
2. Phokha, S., Pinitsoontorn, S., Maensiri, S. & Rujirawat, S. Structure, optical and magnetic properties of $LaFeO_3$ nanoparticles prepared by polymerized complex method. *J. Sol Gel Sci. Technol.* **71**, 333–341. https://doi.org/10.1007/s10971-014-3383-8 (2014).
3. Enhessari, M., Salehabadi, A., Khoobi, A. & Amiri, R. Kinetic properties and structural analysis of $LaCrO_3$ nanoparticles. *Mater. Sci. Pol.* **35**(2), 368–373. https://doi.org/10.1515/msp-2017-0043 (2017).
4. Mitra, A. et al. Simultaneous enhancement of magnetic and ferroelectric properties of $LaFeO_3$ by co-doping with Dy^{3+} and Ti^{4+}. *J. Alloys Compd.* **726**, 1195–1204. https://doi.org/10.1016/j.jallcom.2017.08.074 (2017).
5. Gao, P., Gratzel, M. & Nazeeruddin, M. K. Organohalide lead perovskites for photovoltaic applications. *Energy Environ. Sci.* **7**(8), 2448–2463. https://doi.org/10.1039/c4ee00942h (2014).

6. Zhang, Y. C. et al. A promising supercapacitor electrode material of $CuBi_2O_4$ hierarchical microspheres synthesized via a coprecipitation route. *J. Alloys Compd.* **484**, 707–713. https://doi.org/10.1016/j.jallcom.2016.05.201 (2016).
7. Takalkar, G., Bhosale, R. & AlMomani, F. Combustion synthesized $A_{0.5}Sr_{0.5}MnO_{3-\delta}$ perovskites (where, a = La, Nd, Sm, Gd, Tb, Pr, Dy, and Y) as redox materials for thermochemical splitting of CO_2. *Appl. Surf. Sci.* **489**, 80–91. https://doi.org/10.1016/j.apsusc.2019.05.284 (2019).
8. Dumitru, R. et al. Lanthanum ferrite ceramic powders: Synthesis, characterization and electrochemical detection application. *Materials* **13**(9), 2061. https://doi.org/10.3390/ma13092061 (2020).
9. Choi, J. J. & Billinge, S. J. L. Perovskites at the nanoscale: From fundamentals to applications. *Nanoscale* **8**(12), 6206–6208. https://doi.org/10.1039/c6nr90040b (2016).
10. Phan, T. T. N., Nikoloski, A. N., Bahri, P. A. & Li, D. Facile fabrication of perovskite-incorporated hierarchically mesoporous/macroporous silica for efficient photoassisted-Fenton degradation of dye. *Appl. Surf. Sci. Adv.* **491**, 488–496. https://doi.org/10.1016/j.apsusc.2019.06.133 (2019).
11. Dohnalova, Z., Sulcova, P. & Trojan, M. Synthesis and characterization of $LnFeO_3$ pigments. *J. Therm. Anal. Calorim.* **91**, 559–563 (2008).
12. Shaterian, M., Khoobi, A., Enhessari, M. & Ozaee, K. A new strategy based on thermodiffusion of ceramic nanopigments into metal surfaces and formation of anti-corrosion coatings. *Microporous Mesoporous Mater.* **218**, 62–68. https://doi.org/10.1016/j.micromeso.2015.06.039 (2015).
13. Liu, H. et al. Electrocatalytic reduction of O_2 and H_2O_2 by adsorbed cobalt tetramethoxyphenyl porphyrin and its application for fuel cell cathodes. *J. Power Sources* **161**(2), 743–752. https://doi.org/10.1016/j.jpowsour.2006.04.132 (2006).
14. Marco, J. F. et al. Characterization of the nickel cobaltite, $NiCo_2O_4$, prepared by several methods: An XRD, XANES, EXAFS and XPS. *Study Solid State Chem.* **153**(1), 74–81. https://doi.org/10.1006/jssc.2000.8749 (2000).
15. Gao, Y. Y., Cao, D. X., Wang, G. L. & Yin, C. L. Catalytic behavior of $NiCo_2O_4$ for H_2O_2 electroreduction in alkaline medium. *Acta Phys. Chim. Sin.* **26**(1), 29–33 (2010).
16. Yuan, C. et al. Ultrathin mesoporous $NiCo_2O_4$ nanosheets supported on Ni foam as advanced electrodes for supercapacitors. *Adv. Funct. Mater.* **22**, 4592–4597. https://doi.org/10.1002/adfm.201200994 (2012).
17. Yuan, C. et al. Facile template-free synthesis of capacitors. *J. Mater. Chem.* **22**, 16084–16090. https://doi.org/10.1039/C2JM32351F (2012).
18. Liu, M.-C. et al. A sol–gel process for the synthesis of $NiCo_2O_4$ having improved specific capacitance and cycle stability for electrochemical capacitors. *J. Electrochem. Soc.* **159**(8), A1262–A1266. https://doi.org/10.1149/2.057208jes (2012).
19. Hu, L., Wu, L., Liao, M. & Fang, X. High-performance $NiCo_2O_4$ nanofilm photodetectors fabricated by an interfacial self-assembly strategy. *Adv. Mater.* **23**(17), 1988–1992. https://doi.org/10.1002/adma.201004109 (2011).
20. Jang, K. et al. Synthesis of $NiCo_2O_4$ nanostructures and their electrochemial properties for glucose detection. *Nanomaterials* **11**(1), 55. https://doi.org/10.3390/nano11010055 (2021).
21. Wang, J., Zhang, H., Hu, Z. & Li, J. Tribological properties and lubrication mechanism of nickel nanoparticles as an additive in lithium grease. *Nanomaterials (Basel)* **12**(13), 2287. https://doi.org/10.3390/nano12132287 (2022).
22. Zhan, J., Cai, M., Zhang, C. & Wang, J. Synthesis of mesoporous $NiCo_2O_4$ fibers and their electrocatalytic activity on direct oxidation of ethanol in alkaline media. *Electrochim. Acta* **154**, 70–76. https://doi.org/10.1016/j.electacta.2014.12.078 (2015).
23. Anh, N. T. et al. An on-site and portable electrochemical sensing platform based on spinel zinc ferrite nanoparticles for the quality control of paracetamol in pharmaceutical samples. *Nanoscale Adv.* **6**, 256. https://doi.org/10.1039/d3na00749a (2024).
24. Nguyen, V.-C. & Kim, H. C. Spinel nanoparticles $ZnCo_2O_4$ as high performance electrocatalyst for electrochemical sensing antibiotic chloramphenicol. *J. Electrochem. Sci. Technol.* **15**(1), 152–160. https://doi.org/10.33961/jecst.2023.00486 (2024).
25. Basiri, F. & Taei, M. Application of spinel-structured $MgFe_2O_4$ nanoparticles for simultaneous electrochemical determination diclofenac and morphine. *Microchim. Acta* **184**, 155–162. https://doi.org/10.1007/s00604-016-1995-0 (2017).
26. Madhaiyan, R. et al. Fabrication of spinel $NiCo_2O_4$ nanoflowers by simple hydrothermal method for effective electrochemical detection of NO_2^- in processed food sample. *Food Chem.* **480**, 143964. https://doi.org/10.1016/j.foodchem.2025.143964 (2025).
27. Teodosiu, C., Gilca, A. F., Barjoveanu, G. & Fiore, S. Emerging pollutants removal through advanced drinking water treatment: A review on processes and environmental performances assessment. *J. Clean. Prod.* **197**(1), 1210–1221. https://doi.org/10.1016/j.jclepro.2018.06.247 (2018).
28. O'Flynn, D. et al. A review of pharmaceutical occurrence and pathways in the aquatic environment in the context of a changing climate and the COVID-19 pandemic. *Anal. Methods* **13**, 575–594. https://doi.org/10.1039/D0AY02098B (2021).
29. Motoc, S., Manea, F., Baciu, A., Orha, C. & Pop, A. Electrochemical method for ease determination of sodium diclofenac trace levels in water using graphene-multi-walled carbon nanotubes paste electrode. *Int. J. Environ. Res. Public Health* **19**, 29. https://doi.org/10.3390/ijerph19010029 (2022).
30. Anwar, A. A. A., Mahmoud, R., Abd El-Fatah, G., Farghali, A. A. & Hassouna, M. E. M. Electrochemical determination of diclofenac sodium using modified carbon paste electrode-based Zn/Fe-PANI and its efficient removal using three different layered double hydroxides. *Int. J. Environ. Anal. Chem.* **104**, 9454–9473. https://doi.org/10.1080/03067319.2023.2233913 (2023).
31. Smith, A. T., Anna, M. L. C., Songshan, Z., Bin, L. & Luyi, S. Synthesis, properties, and applications of graphene oxide/reduced graphene oxide and their nanocomposites. *Nano Mater. Sci.* **1**(1), 31–47. https://doi.org/10.1016/j.nanoms.2019.02.004 (2019).
32. Silwana, B., Van Der Horst, C., Iwuoha, E. & Somerset, V. A brief review on recent developments of electrochemical sensors in environmental application for PGMs. *J. Environ. Sci. Health A Tox. Hazard Subst. Environ. Eng.* **51**(14), 1233–1247. https://doi.org/10.1080/10934529.2016.1212562 (2016).
33. Almbrok, E. M., Yusof, N. A., Abdullah, J. & Zawawi, R. M. Electrochemical behavior and detection of diclofenac at a microporous Si_3N_4 membrane modified water–1, 6-dichlorohexane interface system. *Chemosensors* **8**(1), 11. https://doi.org/10.3390/chemosensors8010011 (2020).
34. Yu, H., Jiao, J., Li, Q. & Li, Y. Electrochemical determination of diclofenac sodium in pharmaceutical sample using copper nanoparticles/reduced graphene oxide modified glassy carbon electrode. *Int. J. Electrochem.* **16**, 211024. https://doi.org/10.20964/2021.10.19 (2021).
35. Bansod, B., Kumar, T., Thakur, R., Rana, S. & Singh, I. A review on various electrochemical techniques for heavy metal ions detection with different sensing platforms. *Biosens. Bioelectron.* **94**, 443–455. https://doi.org/10.1016/j.bios.2017.03.031 (2017).
36. Boumya, W. et al. Electrochemical sensors and biosensors for the determination of diclofenac in pharmaceutical, biological and water samples. *Talanta Open* **3**, 100026. https://doi.org/10.1016/j.talo.2020.100026 (2021).
37. Ferrari, A. G. M., Carrington, P., Rowley-Neale, S. J. & Banks, C. E. Recent advances in portable heavy metal electrochemical sensing platforms. *Environ. Sci. Water Res. Technol.* **6**, 2676–2690. https://doi.org/10.1039/D0EW00407C (2020).
38. Kimmel, D. W., Leblanc, G., Meschievitz, M. E. & Cliffel, D. E. Electrochemical sensors and biosensors. *Anal. Chem.* **84**, 685–707. https://doi.org/10.1021/ac202878q (2012).
39. Nagabooshanam, S. et al. Electrochemical micro analytical device interfaced with portable potentiostat for rapid detection of chlorpyrifos using acetylcholinesterase conjugated metal organic framework using Internet of things. *Sci. Rep.* **9**, 19862 (2019).
40. Mollaei, M., Ghoreishi, S. M. & Khoobi, A. Electrochemical investigation of a novel surfactant for sensitive detection of folic acid in pharmaceutical and biological samples by multivariate optimization. *Measurement* **145**, 300–310. https://doi.org/10.1016/j.measurement.2019.05.064 (2019).

41. Ghoreishi, S. M., Behpour, M., Khoobi, A. & Moghadam, Z. Determination of trace amounts of sulfamethizole using a multi-walled carbon nanotube modified electrode: Application of experimental design in voltammetric studies. *Anal. Lett.* **46**(2), 323–339. https://doi.org/10.1080/00032719.2012.718831 (2013).
42. Khoobi, A., Ghoreishi, S. M., Masoum, S. & Behpour, M. Multivariate curve resolution-alternating least squares assisted by voltammetry for simultaneous determination of betaxolol and atenolol using carbon nanotube paste electrode. *Bioelectrochemistry* **94**, 100–107. https://doi.org/10.1016/j.bioelechem.2013.04.002 (2013).
43. Khoobi, A., Attara, A. M., Yousofi, M. & Enhessari, M. A sensitive lead titanate nano-structured sensor for electrochemical determination of pentoxifylline drug in real samples. *J. Nanostruct. Chem.* **9**, 29–37. https://doi.org/10.1007/s40097-019-0295-8 (2019).
44. Dumitru, R. et al. Synthesis, characterization of nanosized $CoAl_2O_4$ and its electrocatalytic activity for enhanced sensing application. *J. Therm. Anal. Calorim.* **128**, 1305–1312. https://doi.org/10.1007/s10973-016-6045-y (2017).
45. Guzman, M. F. et al. Optimization of a differential pulse voltammetric methodology for the quantification of diclofenac using paste electrodes and carbon nanotubes. *ECS Trans.* **76**, 9. https://doi.org/10.1149/07601.0009ecst (2017).
46. Jiokeng, S. L., Tonle, I. K. & Walcarius, A. Amino-attapulgite/mesoporous silica composite films generated by electro-assisted self-assembly for the voltammetric determination of diclofenac. *Sens. Actuators B Chem.* **287**, 296–305. https://doi.org/10.1016/j.snb.2019.02.038 (2019).
47. Nia, N. A., Foroughi, M. M., Jahani, S., Zandi, M. S. & Rastakhiz, N. Fabrication of a new electrochemical sensor for simultaneous determination of codeine and diclofenac using synergic effect of feather-type La^{3+}-ZnO nano-flower. *J. Electrochem. Soc.* **166**, B489–B497. https://doi.org/10.1149/2.1051906jes (2019).
48. Sathisha, A. & Swamy, B. E. K. Simultaneous electrochemical determination of paracetamol, dopamine and diclofenac at diacerein modified carbon paste electrode: A voltammetric study. *Anal. Bioanal. Electrochem.* **10**, 1437–1448 (2018).
49. Wysoczanski, A. & Voigtman, E. Receiver operating characteristic-curve limits of detection. *Spectrochim. Acta B* **100**, 70–77. https://doi.org/10.1016/j.sab.2014.08.005 (2014).
50. Dumitru, R. et al. Mesoporous cobalt ferrite: A rival of platinum catalyst in methane combustion reaction. *Appl. Catal. A Gen.* **467**, 178–186. https://doi.org/10.1016/j.apcata.2013.07.013 (2013).
51. Birzescu, M., Niculescu, M., Dumitru, R., Carp, O. & Segal, E. Synthesis, structural characterization and thermal analysis of the cobalt(II) oxalate obtained through the reaction of 1,2-ethanediol with $Co(NO_3)_2 \cdot 6H_2O$. *J. Therm. Anal. Calorim.* **96**, 979–986. https://doi.org/10.1007/s10973-009-0054-z (2009).
52. Selvaraj, S., Moon, H. & Kim, D. H. Combined effect of nano-structured $NiCo_2S_4$ coated hematite photoanodes for efficient photoelectrochemical water oxidation. *Catal. Today* **347**, 63–69. https://doi.org/10.1016/j.cattod.2018.05.045 (2020).
53. Li, X. et al. Insight of synergistic effect of different active metal ions in layered double hydroxides on their electrochemical behaviors. *Electrochim. Acta* **253**, 302–310. https://doi.org/10.1016/j.electacta.2017.09.075 (2017).
54. Faid, A. Y. & Ismail, H. Highly active and easily fabricated $NiCo_2O_4$ nanoflowers for enhanced methanol oxidation. *Chem. Sel.* **4**(27), 7896–7903. https://doi.org/10.1002/slct.201901580 (2019).
55. Kong, W., Lu, C., Zhang, W., Pu, J. & Wang, Z. Homogeneous core–shell $NiCo_2S_4$ nanostructures supported on nickel foam for supercapacitors. *J. Mater. Chem.* **3**(23), 12452–12460. https://doi.org/10.1039/C5TA02432C (2015).
56. Lenglet, M., Guillamet, R., Dürr, J., Gryffroy, D. & Vandenberghe, R. E. Electronic structure of $NiCo_2O_4$ by XANES, EXAFS and ^{61}Ni Mössbauer studies. *Solid State Commun.* **74**(10), 1035–1039. https://doi.org/10.1016/0038-1098(90)90705-G (1990).
57. Ndione, P. F. et al. Control of the electrical properties in spinel oxides by manipulating the cation disorder. *Adv. Funct. Mater.* **24**, 610–618. https://doi.org/10.1002/adfm.201302535 (2014).
58. Shi, X., Bernasek, S. L. & Selloni, A. Formation, electronic structure, and defects of Ni substituted spinel cobalt oxide: A DFT + U study. *J. Phys. Chem. C* **120**, 14892–14898. https://doi.org/10.1021/acs.jpcc.6b03096 (2016).
59. Chang, T.-C. et al. The effect of degrees of inversion on the electronic structure of spinel $NiCo_2O_4$: A density functional theory study. *ACS Omega* **6**(14), 9692–9699. https://doi.org/10.1021/acsomega.1c00295 (2021).
60. Djara, R. et al. Self-supported electrocatalysts derived from nickel–cobalt modified polyaniline polymer for H_2-evolution and O_2-evolution reactions. *Chem. Cat. Chem.* **12**(22), 5789–5796. https://doi.org/10.1002/cctc.202001235 (2020).
61. Hamdedeina, A. et al. Synthesis and characterization of Ni/$NiCo_2O_4$ modified electrode for methanol electro-catalytic oxidation. *IOP Conf. Ser. Mater. Sci. Eng.* **1046**, 012027. https://doi.org/10.1088/1757-899X/1046/1/012027 (2021).
62. Wang, Z., Xiao, X., Zhang, G., Zhu, Y. & Wang, Y. Electrocatalytic performance of mesoporous $NiCo_2O_4$ nanosheets with elemental electron synergy towards direct glucose in alkaline solution. *J. Phys. Chem. Solids* **167**, 110784. https://doi.org/10.1016/j.jpcs.2022.110784 (2022).
63. Fan, Z. et al. Preparation and capacitive properties of cobalt–nickel oxides/carbon nanotube composites. *Electrochim. Acta* **52**, 2959–2965. https://doi.org/10.1016/j.electacta.2006.09.029 (2007).
64. Asgari, M., Maragheh, M. G., Davarkhah, R., Lohrasbi, E. & Golikand, A. N. Electrocatalytic oxidation of methanol on the nickel–cobalt modified glassy carbon electrode in alkaline medium. *Electrochim. Acta* **59**, 284–289. https://doi.org/10.1016/j.electacta.2011.10.091 (2012).
65. Laviron, E. General expression of the linear potential sweep voltammogram in the case of diffusionless electrochemical systems. *J. Electroanal. Chem.* **101**, 19–28. https://doi.org/10.1016/S0022-0728(79)80075-3 (1979).
66. Mekassa, B., Baker, P. G. L., Chandravanshi, B. S. & Tessema, M. Synthesis, characterization, and preparation of nickel nanoparticles decorated electrochemically reduced graphene oxide modified electrode for electrochemical sensing of diclofenac. *J. Solid State Electrochem.* **22**, 3607–3619. https://doi.org/10.1007/s10008-018-4071-3 (2018).

Acknowledgements

This work was partially carried out through the "Nucleu" Program within the National Research Development and Innovation Plan 2022–2027 with the support of Romanian Ministry of Research, Innovation and Digitalization, Contract No. 3N/2022, Project code PN 23 22 01 01 and partially by a grant of the "Program intern de stimulare si recompensare a activitatii didactice", contract number 10161/11 June 2021

Author contributions

R.D. (V.) synthesized $NiCo_2O_4$; L.F.P., S.N., S.M. investigated the electrochemical characterization of electrode materials; A.P. and F.M. tested and developed the electrochemical detection methods. V.A.S., A.C.I. investigated morpho-structural characterization by XRD Rietveld refinement and SEM; B.S.V. investigated morpho-structural characterization by TEM/HRTEM/SAED/STEM-EDX; A. M. P. provided XPS investigations; R.D.(V.), L.F.P., F.M. and A.C.I. wrote the main manuscript text. All authors reviewed the manuscript.

Declarations

Competing interests
The authors declare no competing interests.

Additional information
Supplementary Information The online version contains supplementary material available at https://doi.org/10.1038/s41598-025-07722-y.

Correspondence and requests for materials should be addressed to F.M. or R.D.

Reprints and permissions information is available at www.nature.com/reprints.

Publisher's note Springer Nature remains neutral with regard to jurisdictional claims in published maps and institutional affiliations.